Orbital ordering, Jahn-Teller distortion, and resonant x-ray scattering in $KCuF_3$

N. Binggeli
Abdus Salam International Center for Theoretical Physics and INFM DEMOCRITOS National Simulation Center, Strada Costiera 11, 34014 Trieste, Italy

M. Altarelli
Sincrotrone Trieste, Area Science Park, 34012 Basovizza, Trieste and Abdus Salam International Center for Theoretical Physics, 34014 Trieste, Italy

(Received 12 March 2004; published 31 August 2004)

The orbital, lattice, and spin ordering phenomena in $KCuF_3$ are investigated by means of local-density-approximation plus onsite-Coulomb interaction (LDA+U) calculations, based on *ab initio* pseudopotentials. We examine the Cu 3*d* orbital ordering and the associated Jahn-Teller distortion in several different spin-ordered structures of $KCuF_3$. The ground state is correctly predicted to be an A-type antiferromagnetic structure, and the calculated Jahn-Teller distortion agrees also well with experiment. Concerning the orbital ordering, we find that even for a highly ionic compound such as $KCuF_3$, the orbital-order parameter is significantly reduced with respect to its nominal value due to Cu(3*d*)−F(2*p*) hybridization. We also calculate the Cu *K*-edge resonant x-ray scattering spectra for Bragg reflections associated with orbital order. Consistent with previous studies, we find that the resonant signal is dominated by the structural anisotropy in the distribution of the F neighbors of the resonant Cu atom, and that the Cu 3*d* orbital ordering has only a minor influence on the spectra. Our LDA+U results, however, also indicate that a change in the magnetic structure has a small influence on the Jahn-Teller distortion, and hence on the resonant spectrum, in the conventional (room-temperature) crystallographic structure of $KCuF_3$. This may indicate that the large change observed experimentally in the resonant signal near the Néel temperature is related to a low-temperature structural transformation in $KCuF_3$.

DOI: 10.1103/PhysRevB.70.085117 PACS number(s): 71.20.−b, 71.70.Ch, 78.70.Ck

I. INTRODUCTION

The pseudocubic perovskite $KCuF_3$ is a magnetic insulator that has attracted significant interest since the 1960s, as a prototype material for orbital ordering, cooperative Jahn-Teller distortion, and low-dimensional magnetism.[1–3] $KCuF_3$ is also structurally related to high-T_c superconducting cuprates and colossal-magnetoresistance manganites. In recent years, renewed attention has been given to the problem of orbital ordering and to the study of the interactions between orbital, magnetic, and structural ordering in strongly correlated 3*d*-transition-metal compounds, stimulated in large part by the interest in colossal-magnetoresistance manganites.[4] In the latter systems, the interplay between orbital, charge, spin, and lattice degrees of freedom is known to play an essential role in establishing the observed physical properties. Contrary to the case of charge, spin, and lattice ordering, however, which can be investigated by conventional x-ray, neutron, and electron diffraction techniques, direct experimental observation of orbital ordering has been—and remains in most cases—a challenge.

Recently, resonant elastic x-ray scattering (RXS) techniques have been developed to probe orbital ordering. RXS has been applied to a number of orbitally ordered compounds, including various manganites[5,6] and $KCuF_3$.[7,8] Except for very recent measurements carried out on layered/doped manganites at the Mn $L_{2,3}$ edges,[9–12] most of the experiments performed to date have used excitations from the transition-metal 1*s* core level, i.e., *K*-edge excitations. In the case of $KCuF_3$ and for related perovskite manganites such as $LaMnO_3$, the *K* edge excitation is the only possible core-level excitation for which resonant photons have a sufficiently large wave vector to access a Bragg vector of the targeted orbitally ordered structure. The *K*-edge scattering process in manganites and $KCuF_3$, however, derives from virtual electric dipole excitations to empty transition-metal 4*p* states. The resulting RXS amplitude is thus not directly related to the 3*d* states that exhibit orbital ordering, but to the anisotropy induced in the surrounding 4*p* states. Although the latter is due, in principle, to the orbital ordering and/or associated Jahn-Teller distortion, this indirect dependence complicates the interpretation of *K*-edge RXS data. In fact, it has been first proposed that the measured anisotropy is determined by the 3*d* orbital polarization via onsite 3*d*-4*p* Coulomb interaction.[13] However, subsequent local-density-approximation (LDA) calculations and LDA plus onsite-Coulomb interaction (LDA+U) calculations, performed for a number of manganites[14–17] and also for $KCuF_3$,[8,18] have provided rather strong evidence that the *K*-edge scattering amplitude in these systems is mostly sensitive to the Jahn-Teller distortion that accompanies the orbital ordering, rather than to the orbital ordering itself.

In $KCuF_3$, an interesting feature has been observed concerning the temperature dependence of the *K*-edge RXS intensity for orbital Bragg peaks.[7,8] The measured scattering intensity shows a substantial and sudden increase (within 4 to 5 K), with decreasing temperature, when approaching the Néel temperature. A somewhat similar phenomenon has been observed also in $LaMnO_3$ at the *K* edge[5] and in $La_{0.5}Sr_{1.5}MnO_4$ at the $L_{2,3}$ edges,[10] for temperatures ap-

proaching the Néel temperature, but in these systems the changes in the orbital scattering intensity take place over a much wider temperature range, i.e., one to two orders of magnitude wider. These phenomena are therefore not necessarily related, but they are all very puzzling because they take place in a temperature region where both the orbital-order parameter and the Jahn-Teller distortion are expected to be saturated. In all of these systems, the origin of the changes in the scattering intensity is an unresolved issue.

For $KCuF_3$, two different interpretations have been proposed. On one hand, the change in RXS intensity has been ascribed to a change in the orbital order parameter, and interpreted as indicative of a strong coupling between spin and orbital degrees of freedom.[7,8] On the other hand, based on the results of LDA+U calculations showing a dominant influence of the Jahn-Teller distortion on the RXS spectra, the jump in intensity has been attributed to an increase of the Jahn-Teller distortion in the low-temperature magnetic phase.[18] These interpretations are also not necessarily mutually exclusive; a change in the magnetic structure may induce a change in the orbital-order parameter, which in turn may modify the Jahn-Teller distortion. In principle, first-principle calculations could help discriminating between these various possibilities by providing quantitative information on the influence of the magnetic structure on both the Jahn-Teller distortion and the orbital-order parameter. As yet, however, to our knowledge these issues have not been addressed by such calculations for $KCuF_3$.

In the present work, we use state-of-the-art LDA+U calculations, based on *ab initio* pseudopotentials, to investigate the electronic, structural, and magnetic properties of $KCuF_3$. Our main targets are the orbital ordering and Jahn-Teller distortion, and we address the influence of the magnetic structure on these properties. We also evaluate the Cu *K*-edge RXS spectrum, and investigate the influence of the magnetic structure and Jahn-Teller distortion on the simulated spectrum. Unlike other density-functional-related approaches, the LDA+U method has not been extensively used to examine structural properties. In this study we therefore also first demonstrate the ability of LDA+U pseudopotential calculations to provide a realistic description of the ground-state properties of $KCuF_3$, when full structural optimization is performed.

$KCuF_3$ crystallizes in a perovskite structure which is tetragonally distorted by a collective Jahn-Teller distortion of the CuF_6 octahedra. Two different polytypes have been identified experimentally at room temperature, which differ in their atomic-plane stacking along the *c* axis (Fig. 1).[19] The Cu ions in $KCuF_3$ are nominally in a Cu^{2+} (d^9) configuration, with completely filled $3d$-t_{2g} orbitals and one hole in one of the cubic degenerate $3d$-e_g orbitals ($3d_{z^2-x^2}$, $3d_{3y^2-r^2}$). The cubic degeneracy of the e_g states is lifted in the paramagnetic phase, well above room temperature, by an orbital polarization and Jahn-Teller instability. The octahedra elongate along the *a* or *b* principal axes, with an alternate order on neighboring Cu A and B sites in the *ab* plane (see Fig. 1). The distortion corresponds to an alternate distribution of $3d_{z^2-x^2}$ and $3d_{z^2-y^2}$ hole orbitals on Cu A and B sites.[2] Along the *c* axis, the stacking of the planes may be antiferromagneticlike (type *a*) or ferromagneticlike (type *d*), giving rise to the two different polytypes.

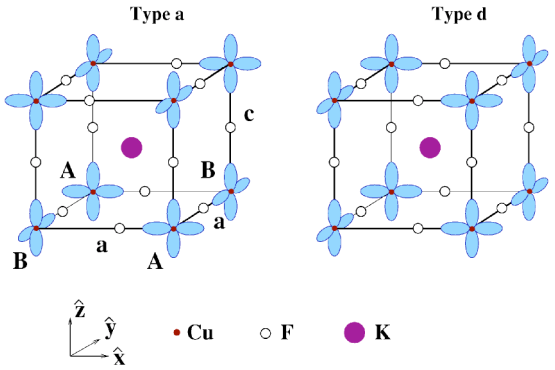

FIG. 1. (Color online) Schematic views of the atomic structure and of the ordering of the Cu $3d$ hole orbitals in the *a*- (left) and *d*- (right) polytypes of $KCuF_3$.

Below the Néel temperature (38 K for polytype *a*, 22 K for polytype *d*), the spins arrange in an A-type antiferromagnetic (AF) structure, with strong AF superexchange interaction between adjacent Cu atoms along the *c* axis, and weak ferromagnetic (FM) superexchange coupling between Cu nearest neighbors within the *ab* plane.[3,20] This magnetic structure is consistent with the predictions of the Goodenough-Kanamori-Anderson[2] rules for the superexchange interactions associated with the orbital-ordered configurations displayed in Fig. 1. Such orbital configurations have been confirmed by previous LDA+U and Hartree-Fock calculations for $KCuF_3$.[8,18,21–23] Previous calculations have also shown that the LDA approach fails to correctly predict the stable orbitally ordered AF insulating structure of $KCuF_3$, while the LDA+U corrects this feature.[21]

In this paper, we concentrate on the *a*-type structure of $KCuF_3$, which has been the focus of the experimental RXS studies.[7,8] The work is organized as follows: In Sec. II, we briefly present the calculation method. In Sec. III we address the structural properties of the low-temperature A-AF structure; the corresponding orbital ordering and electronic properties are examined in Sec. IV. In Sec. V we investigate the energetics and superexchange couplings of several different (meta)-stable spin structures of $KCuF_3$. The influence of the magnetic structure on the orbital ordering and Jahn-Teller distortion is addressed in Sec. VI. In Sec. VII we present our results for the RXS spectra, and we summarize our conclusions in Sec. VIII.

II. METHODOLOGY

The calculations are performed within the LDA+U scheme using the pseudopotential plane-wave method. We employ the rotational invariant[21] LDA+U energy functional:[24,25]

$$E^{\mathrm{LDA+U}}[\rho^{\uparrow},\rho^{\downarrow},\{n_{\lambda}^{I,\uparrow}\},\{n_{\lambda}^{I,\downarrow}\}] = E^{\mathrm{LDA}}[\rho^{\uparrow},\rho^{\downarrow}] + \frac{U-J}{2}\sum_{I,\lambda,\sigma} n_{\lambda}^{I,\sigma}(1-n_{\lambda}^{I,\sigma}), \qquad (1)$$

where $E^{\mathrm{LDA}}[\rho^{\uparrow},\rho^{\downarrow}]$ is the standard LDA energy functional, ρ^{σ} is the electron spin density with spin polarization σ, U (J)

is the onsite Coulomb (exchange) interaction parameter for the localized electrons, the Cu 3*d* electrons, and $n_{\lambda}^{I,\sigma}$ are the occupation numbers of the localized orbitals. I and λ are indexes for atomic sites and orbitals, respectively. The occupation numbers $n_{\lambda}^{I,\sigma}$ are the eigenvalues of the density matrices:

$$n_{m,m'}^{I,\sigma} = \sum_{\boldsymbol{k},i} f_{\boldsymbol{k},i}^{\sigma} \langle \varphi_m^{I,\sigma} | \psi_{\boldsymbol{k},i}^{\sigma} \rangle \langle \psi_{\boldsymbol{k},i}^{\sigma} | \varphi_{m'}^{I,\sigma} \rangle, \tag{2}$$

where $\varphi_m^{I,\sigma}(\boldsymbol{r})$ are the rotational-degenerate atomic orbitals of the localized-*d*-electron shell, m stands for the angular quantum number, $\psi_{\boldsymbol{k},i}^{\sigma}(\boldsymbol{r})$ are the crystal Bloch states, and $f_{\boldsymbol{k},i}^{\sigma}$ are the corresponding occupation numbers.

In our pseudopotential calculations, the crystal Bloch states, $\psi_{\boldsymbol{k},i}^{\sigma}(\boldsymbol{r})$, are represented by Bloch pseudo-wave functions, and the matrix elements $\langle \varphi_m^{I,\sigma} | \psi_{\boldsymbol{k},i}^{\sigma} \rangle$, in Eq. (2), are evaluated by projecting the crystal pseudo-wave functions on atomic pseudo-wave functions.[26] We employ the Perdew-Zunger parameterization of the LDA exchange-correlation potential.[27] For the effective onsite Coulomb interaction parameter, $U_{\mathrm{eff}}=U-J$, we use a value of 6.6 eV. This value corresponds to the calculated values $U=7.5$ eV and $J=0.9$ eV obtained by constrained LDA computations for $KCuF_3$ in Ref. 21.

We employ a Vanderbilt[28] ultrasoft pseudopotential for Cu and norm-conserving Troullier-Martins[29] pseudopotentials for K and F. Some of the calculations have also been performed using a Troullier-Martins pseudopotential for Cu,[29] for comparison. The pseudopotentials we use are scalar relativistic. The Vanderbilt pseudopotential has been generated in the nonmagnetic Cu $3d^{9.5}4s^{0.5}4p^{1}$ atomic configuration, using for the core-cutoff radii: $r_s=2.1$, $r_p=2.2$, and $r_d=2.0$ a.u. The Troullier-Martins pseudopotentials have been generated in the ground-state configuration of the non-spin-polarized atom, with the cutoff radii (in a.u.): $r_{4s}=3.50$, $r_{4p}=r_{3d}=3.75$ for K and $r_{2s}=r_{2p}=1.40$ for F. The Troullier-Martins pseudopotentials have been cast into the Kleinmann-Bylander[30] nonlocal form using the *s* component as a local part. For Cu and K we have included the nonlinear core correction[31] to the exchange-correlation potential to account for the overlap between the valence and core charge; for fluorine this is not necessary, since we treat the F 2*s* semicore electrons as valence electrons.

All calculations are carried out in a 20-atom tetragonal unit cell. We use a kinetic-energy cutoff of 80 Ry for the plane-wave expansion of the electronic states. The integrations in reciprocal space are performed using a (4,4,2) Monkhorst-Pack[32] k-point grid for all structures, except the nonmagnetic structure of $KCuF_3$ which is metallic. For the latter structure we employ a (6,6,4) Monkhorst-Pack grid together with a Gaussian electronic-level broadening scheme,[33] with a full width at half maximum of 0.01 Ry. With the above parameters, the estimated convergence on the relative energies of the various magnetic structures considered in this work is ~1 meV per formula unit.

Concerning the pseudopotentials, we have performed some comparative studies using the Troullier-Martins and Vanderbilt pseudopotential for Cu. They indicate negligible differences, in general, for results concerning the electronic-structure properties. For the structural properties, the Vanderbilt pseudopotential yields a larger (~15% larger) Jahn-Teller distortion, and a smaller equilibrium volume (2% smaller) than the Troullier-Martins pseudopotential. This is related to a higher degree of localization within the core region of the Cu 3*d* pseudo-charge density obtained with the Vanderbilt compared to the Troullier-Martins pseudopotential. The structural trends, however, and in particular the dependence on the magnetic state, are the same with the two types of pseudopotentials. The effect of the K 3*p* and 3*s* semicore electrons has also been investigated. Potassium is known to have semicore states which are rather polarizable. We have therefore performed test calculations treating the K 3*p* and 3*s* electrons as valence electrons. They show that the inclusion of the K semicore electrons has virtually no effect on the electronic properties and changes the equilibrium values of the structural parameters by less than 1%.

TABLE I. Calculated values of the equilibrium lattice constant, a, tetragonal lattice ratio, c/a internal structural parameter, x_F, and bulk modulus, B_0, of $KCuF_3$.

	a(Å)	c/a	x_F	B_0 (GPa)
LDA+U	4.03	0.955	0.2320	75
Expt[a] (10 K)	4.126	0.9486		
Expt[b] (298 K)	4.141	0.9476	0.2280	

[a]Reference 20
[b]Reference 5

III. STRUCTURAL PROPERTIES

In Table I we show our results for the equilibrium lattice constant, a, tetragonal lattice ratio c/a, fluorine coordinate x_F, and bulk modulus B_0 of the low-temperature A-AF structure of $KCuF_3$. The theoretical values of the structural parameters are compared to experimental values at low temperature—when available—and at room temperature. The theoretical equilibrium lattice constant a is about 2% smaller than the measured low-temperature value. This is comparable to LDA results for related perovskite materials, such as the ferroelectric oxides studied in Ref. 34, for which the LDA underestimation of the lattice constant is typically ~1 to 2%.

Our LDA+U values for c/a and x_F agree well with experiment, i.e., to within 1 and 2%, respectively. The calculated relaxed bond lengths for the three inequivalent Cu-F bonds along the x, y and z directions (at a Cu A site) are 1.87, 2.16, and 1.92 Å, respectively, versus 1.88, 2.25, and 1.96 Å in the experiment.[35] The in-plane quadrupolar distortion $\Delta X=(0.25-x_F)2a$, associated with the Jahn-Teller distortion of the CuF_6 octahedra, is 3.6% of a, compared to the experimental value of 4.4%.[35] Hartree-Fock calculations[22] performed for the *d*-type structure yield a distortion $\Delta X/a$ of 2.6%; the same Hartree-Fock calculations corrected *a posteriori* using a gradient-corrected correlation functional give a distortion of 3.4%, closer to our calculated value. Earlier LDA+U calculations, based on the full-potential

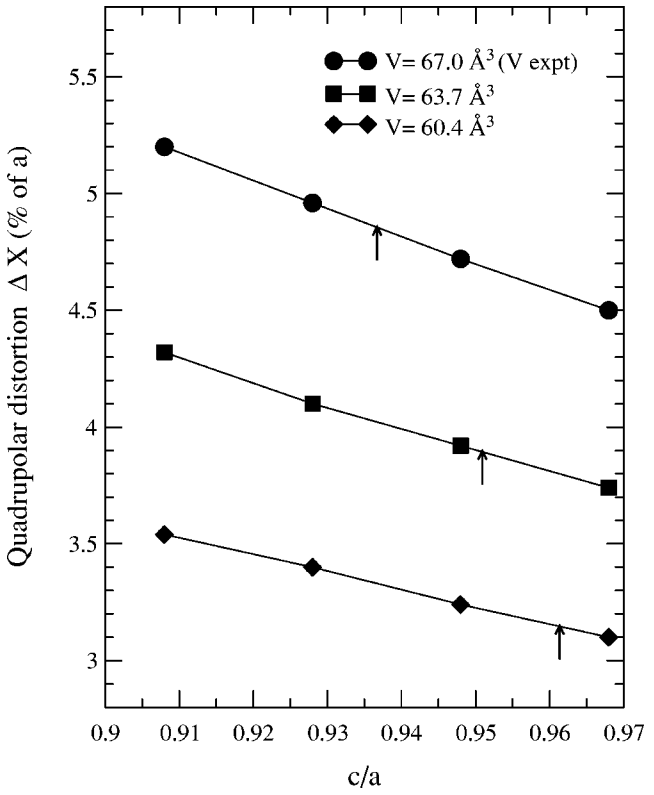

FIG. 2. Calculated quadrupolar distortion $\Delta X=(0.25-x_F)2a$ as a function of the cell-shape ratio c/a for different volumes of $KCuF_3$. The arrows indicate the equilibrium values under hydrostatic conditions.

linear-muffin-tin-orbital method and performed using the experimental values of lattice constants, reported a smaller quadrupolar distortion of 2.5% for the *d*-type structure.[21] To our knowledge, no experimental value is available for the bulk modulus of $KCuF_3$. Our value of 75 GPa, however, is in reasonable agreement with the B_0 value of 84 GPa derived from semiempirical pair-interaction-model calculations for the elastic constants of $KCuF_3$.[36]

The structural optimization needed to determine the parameter values in Table I was carried out considering several different unit-cell volumes, and for each volume several different c/a ratios, and by fully relaxing in each case the F internal coordinates. As a by-product, we have therefore access to the dependence of the quadrupolar distortion on tetragonal strain and also to the hydrostatic-pressure dependence of c/a and x_F. In Fig. 2 we display the calculated equilibrium quadrupolar distortion ΔX as a function of the c/a ratio, for three different volumes (including the experimental one). Consistent with semiempirical model descriptions,[2] an increase in ΔX decreases c/a; the results in Fig. 2 indicate that a 10% increase in ΔX decreases c/a by $\sim$5%. In Table II we also reported the equilibrium values of x_F and c/a at different volumes. Decreasing the volume decreases the quadrupolar distortion and increases the c/a ratio. The latter trend is not inconsistent with the increase in the experimental c/a ratio observed with decreasing temperature (and volume) in Table I.

In the following sections we report our results for the electronic properties, magnetic structure, and RXS spectra of

TABLE II. Calculated equilibrium values of the tetragonal lattice ratio c/a and internal structural parameter x_F of $KCuF_3$ at different volumes.

V (Å^3)	c/a	x_F
67.03	0.937	0.2257
63.68	0.951	0.2305
60.39	0.961	0.2343
57.24	0.968	0.2371

$KCuF_3$ evaluated at the reference experimental values of the structural parameters. We note that using the theoretical values of the structural parameters would not change significantly the results, i.e., produce negligible changes in the orbital-order parameters, variations of $\sim 0.01\mu_B$ in the magnetic moments, and changes of the order of 0.1 eV in the relative energies of the electronic states.

IV. ELECTRONIC STRUCTURE AND ORBITAL ORDERING

In Fig. 3 we present the $KCuF_3$ differential charge density for the A-AF structure, i.e., the difference between the crystal electronic charge density and the superposition of spherical atomic charge densities of neutral atoms. The differential density provides information on the electronic charge rear-

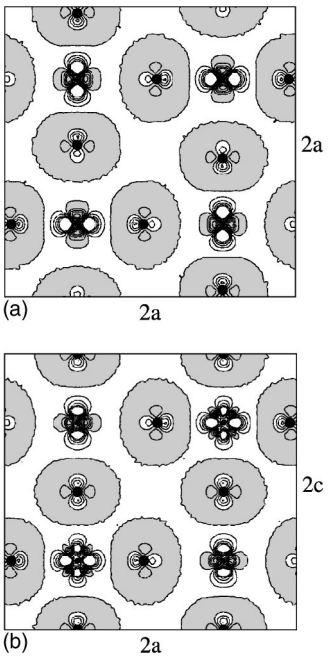

FIG. 3. Difference between the crystal electronic charge density and the superposition of spherical atomic charge densities of neutral atoms in a (001) (panel a) and a (010) (panel b) CuF atomic plane of $KCuF_3$. The positions of the Cu (F) atoms are indicated by small (large) dark disks. Regions of electron accumulation (depletion) are shown in gray (white). Contour lines are separated by $0.03|e|/\text{bohr}^3$; negative electron densities are truncated below $-0.15|e|/\text{bohr}^3$ (near the Cu atoms).

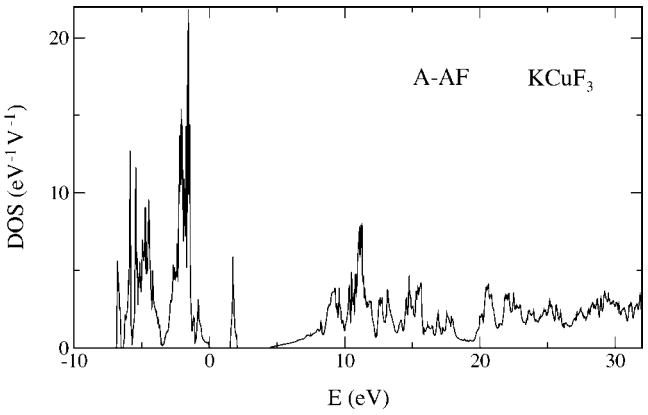

FIG. 4. Electronic density of states of A-AF $KCuF_3$. The zero of energy corresponds to the valence band maximum.

rangements involved in the crystal formation, including charge transfers associated with bond formation and orbital ordering. The differential charge is displayed both in a CuF(001) [Fig. 3(a)] and in a CuF(010) [Fig. 3(b)] atomic plane of $KCuF_3$.

The differential density is clearly partitioned into F-related/Cu(K)-related electron accumulation/depletion regions, consistent with the ionic nature of $KCuF_3$. The Cu 3*d* orbital ordering shows up quite strikingly in the maps, i.e., in the alternate sequence of depleted $d_{z^2-x^2}$- and $d_{z^2-y^2}$-like orbital densities on neighboring Cu A and B sites in Figs. 3(a) and 3(b). We notice a slight asymmetry in the $d_{z^2-x^2}$-like ($d_{z^2-y^2}$-like) orbital density related to the tetragonal distortion of the lattice, i.e., stronger depletions for the lobes along the *x* (respectively *y*) axis than for the lobes along the *z* axis. We also observe a local increase in the electronic density of some of the nominally "filled" Cu 3*d* orbitals—in particular the $d_{3y^2-r^2}$ ($d_{3x^2-r^2}$) orbitals—suggesting a slight contraction of the 3*d* states of the Cu ion in the crystal with respect to those of the isolated atom. We note that the relaxation of the three inequivalent Cu–F bonds follows the trend of decreasing bond length with increasing Cu 3*d* localized-hole charge on the bond, as expected from electrostatic interaction with the F anions.

The differential maps indicate a significant interaction (hybridization) between Cu 3*d* e_g and F $2p_\sigma$ states and a related non-negligible delocalization of the Cu hole on the nearest-neighbor F $2p_\sigma$ states. These features, together with the deviation from purely $d_{z^2-x^2}$ ($d_{z^2-y^2}$) hole orbitals, suggest a somewhat incomplete z^2-x^2/z^2-y^2 orbital ordering. To be more quantitative in this statement, we have evaluated, from the density matrix, the total number of 3*d* holes per Cu site, $n_{3d}^{\text{hole}}=10-\Sigma_{\sigma,\lambda}\, n_\lambda^\sigma$, and the expectation value of the number of holes in the $d_{z^2-x^2}$ orbital on an A site (or equivalently, $d_{z^2-y^2}$ orbital on a B site), $\overline{n}_{z^2-x^2}^{A,\text{hole}}=2-\Sigma_\sigma\, n_{z^2-x^2,z^2-x^2}^{A,\sigma}$. We note that the occupation numbers we obtain from the density matrix for the t_{2g} orbitals are identically 1.00 per spin, so that the total number of 3*d* holes is identical to the number of e_g holes in our calculations. The calculated values are $n_{3d}^{\text{hole}}=n_{e_g}^{\text{hole}}=0.63$ and $\overline{n}_{z^2-x^2}^{A,\text{hole}}=0.61$. Hence, the degree of z^2-x^2/z^2-y^2 orbital ordering, measured by $\overline{n}_{z^2-x^2}^{A,\text{hole}}$, is significantly reduced (by 39%) with respect to its nominal value of one. Most of this reduction, however, can be accounted for by the decrease in the number of e_g hole, $n_{e_g}^{\text{hole}}$, relative to one (37%), and derives thus from the delocalization of the 3*d* hole (due to hybridization) on neighboring F orbitals. The $d_{z^2-x^2}$ ($d_{z^2-y^2}$) character of the ordered orbitals on the A (B) sites, measured by the ratio $\overline{n}_{z^2-x^2}^{A,\text{hole}}/n_{e_g}^{\text{hole}}$, is instead nearly complete [i.e., 97% of the $d_{z^2-x^2}$ ($d_{z^2-y^2}$) type].

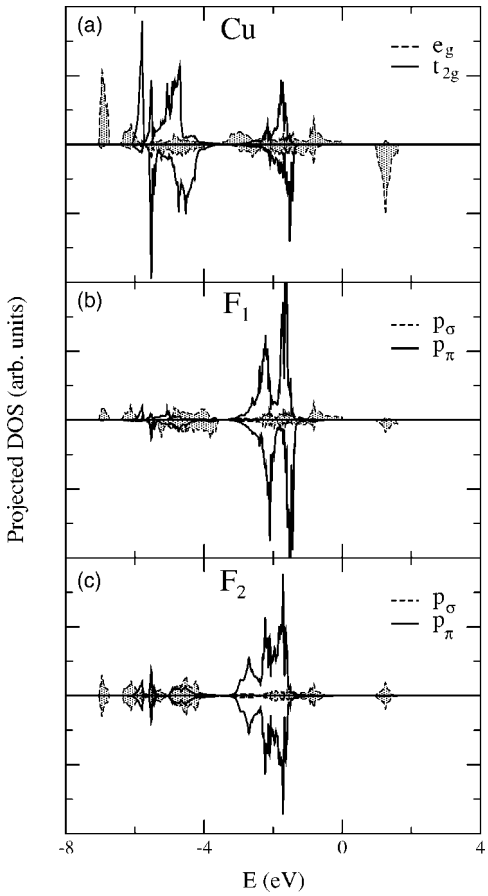

FIG. 5. Projected Cu 3*d* and F 2*p* atomic densities of states in $KCuF_3$. Density of states projected onto: (a) the Cu 3*d* e_g (dashed line) and t_{2g} (solid line) orbitals, (b) the F_1, and (c) the F_2 $2p_\sigma$ (dashed line) and $2p_\pi$ (solid line) orbitals. In each panel, the upper half corresponds to the majority spin states and the lower half to the minority spin states. The zero of energy corresponds to the valence band maximum.

The calculated electronic density of states (DOS) of A-AF $KCuF_3$ is shown in Fig. 4. $KCuF_3$ is an insulator in our calculations with a gap of 1.54 eV. The valence DOS of $KCuF_3$ exhibits two main structures: a low-energy structure (−7 to −3.5 eV), which includes mostly Cu 3*d* states, with an admixture of F 2*p* states (mainly $2p_\sigma$ states), and a high-energy structure (−3.5 to 0 eV), which is dominated by F 2*p* states, and includes also a non-negligible contribution from Cu 3*d* states. The corresponding projected Cu 3*d* and F 2*p* atomic DOS are displayed in Fig. 5.[37] The Cu 3*d* local atomic DOS has been split into contributions from the t_{2g} and e_g states [Fig. 5(a)] and the F 2*p* local DOS into contributions from the p_σ and p_π orbitals on each of the two inequivalent F sites [Figs. 5(b) and 5(c)]. The sharp lowest-

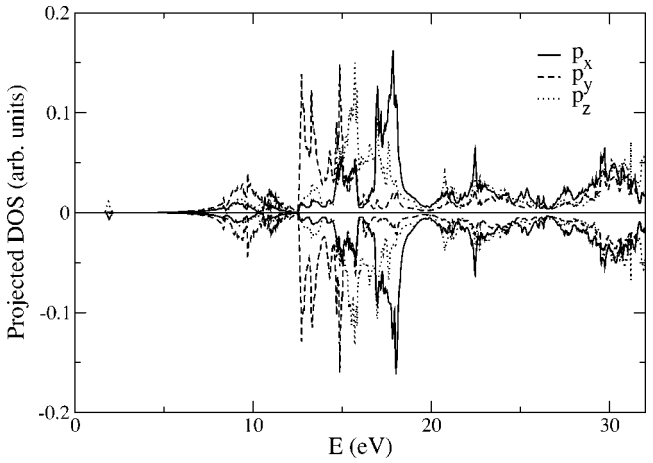

FIG. 6. Density of states projected onto the Cu $4p_x$ (solid line), $4p_y$ (dashed line), and $4p_z$ (dotted line) orbitals at a Cu A site.

energy conduction-band feature, in Fig. 4, clearly derives from the ordered Cu e_g empty orbitals that have the minority spin on each Cu site [see Fig. 5(a)]. Within the LDA+U scheme, the lowest-energy conduction-band feature may be viewed as the upper Hubbard band associated with the localized e_g orbitals illustrated in Fig. 1, the corresponding lower Hubbard band being the sharp lowest-energy valence-band feature in Fig. 5(a). The existence of a significant hybridization between Cu e_g and F p_σ states, in Fig. 5, is apparent from the energy degeneracies and analogous dispersions of the related features. Inspection of Fig. 5 also reveals a nonnegligible interaction between Cu t_{2g} and F p_π states.

At higher energy, in Fig. 4, one finds a second conduction-band edge (at about 5 eV) associated with K 4*s* states, with also a contribution from Cu 4*s* states. The two sharp features located at ~9 and 11 eV, in Fig. 4, originate from K 3*d* states. We note that the Cu 4*p* states, which are the intermediate states in the Cu *K*-edge RXS process, contribute to the DOS over a large energy region that ranges from about 8 to 32 eV (at least). The corresponding Cu $4p_x$, $4p_y$, and $4p_z$ projected densities of states are represented in Fig. 6 (for a Cu A site). The dominant features of the Cu $4p_x$ and $4p_y$ densities of states exhibit a splitting of about 6 eV produced by the F quadrupolar distortion ΔX. The inward/outward relaxation of the nearest-neighbor F anions along the x/y axis tends to shift the $4p_x/4p_y$ states at higher/lower energy with respect to the $4p_z$ states. It should be noted, concerning the high-energy unoccupied states occurring above 5 eV, that—unlike the lower-energy unoccupied Cu $d_{z^2-x^2}$ states associated with the sharp feature—these states are totally insensitive to the effective Hubbard term, U_{eff}, in our LDA+U calculations. These states are thus expected to suffer from the usual LDA underestimation of the gap (i.e., to be shifted to lower energy with respect to quasiparticle energies obtained in GW calculations).

V. MAGNETIC STRUCTURES

The Goodenough-Kanamori-Anderson (GKA) rules predict,[2] for the half-filled-$d_{z^2-x^2}/d_{z^2-y^2}$ orbital configurations

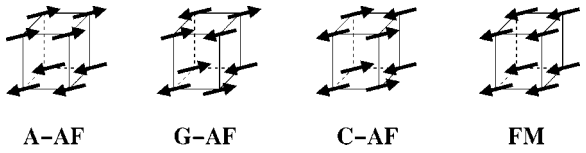

FIG. 7. Magnetic structures considered in this work for $KCuF_3$.

displayed in Fig. 1, that the favorable Cu superexchange interactions should be antiferromagnetic and strong along the *c* axis, and weakly ferromagnetic within the *ab* plane. In order to probe the magnetic interactions in our system, and also to address the influence of the magnetic order on the electronic and structural properties (in the next section), we have considered several different possible (meta)-stable spin configurations for $KCuF_3$, illustrated in Fig. 7. In addition to the A-AF structure, we have considered the AF G- and C-type configurations, the FM state, and also the nonmagnetic (NM) configuration.

In Table III we give the relative energies of the various spin structures together with the corresponding values of the ordered Cu spin moment m_s, computed as the integrated absolute value of the magnetic moment per Cu atom. In agreement with experiment, and consistent with the GKA rules, the A-AF structure is the most stable configuration. The second-most stable configuration is the G-AF spin structure, where the AF order is preserved within the Cu chains along the *c* axis, but FM order has been replaced by AF order within the *ab* plane. The structures having, instead, FM order within the Cu *c* chains (C-AF and FM in Fig. 7) are energetically much less competitive. For the latter structures, we note that AF spin order is more favorable than FM spin order within the *ab* plane (E[C-AF]<E[FM]). This is contrary to the situation observed for the structures having AF spin order within the chains, where FM order is preferred within the *ab* plane (E[A-AF]<E[G-AF]). With the exception of the E[C-AF]<E[FM] case, the energy ordering we find is consistent with the trend expected from the GKA rules for half-filled orbitals. Concerning the (E[C-AF]<E[FM]) anomaly, we note that in our system the hole orbital occupation differs from the half-filled situation (see also next section), and for the weak superexchange interaction within the *ab* plane, such a deviation can change the sign of the superexchange coupling.

The energy of the NM structure, in Table III, is by far (0.2 to 0.3 eV) the largest of all. It should be noted, however, that

TABLE III. Calculated total energies and ordered Cu spin moments in the various magnetic structures of $KCuF_3$ considered in this work. Energies are given per formula units and measured relative to the energy of the A-AF structure.

	E (meV)	m_s (μ_B)
A-AF	0	0.91
G-AF	10	0.90
C-AF	58	0.98
FM	70	1.03
NM	297	0

a large fraction of the energy difference between the NM structure and the stable A-AF phase can be accounted for by the energy change of an isolated Cu^{2+} ion when its configuration is switched from non-spin polarized to spin polarized [i.e., +0.24 eV in our LDA atomic calculations for a spin moment of 0.95 μ_B (see Table III)]. For the paramagnetic phase, thus with disordered spins on the different Cu sites, a reasonable energy estimate would be E[NM] −0.24 eV $\approx$0.06 eV, which is intermediate between the energy of the FM and A-AF phase.

We note that the relative stability of the different structures, in Table III, is reflected in their band gaps. We find that the band gap changes from 1.54 eV, for the A-AF structure, to 1.47, 1.00, 0.72, and 0 eV for the G-AF, C-AF, FM, and NM structures, respectively.

In Table III, the ordered moment m_s of a Cu with a given spin σ increases, in the different spin structures, with increasing number of Cu nearest neighbors along the *c* axis having the same spin σ. We also observe an increase in the moment, but significantly smaller, with increasing number of nearest neighbors having the same spin within the *ab* plane. These trends are consistent with the expected Cu–F–Cu spin-density overlaps associated with the orbital arrangements in Fig. 1. The experimental value of the Cu ordered spin moment measured by neutron diffraction in the A-AF structure at low temperature (4 K) is $\sim 0.49\mu_B$,[3] which is significantly smaller than our value of $0.91\mu_B$. The small experimental m_s in $KCuF_3$, however, is generally attributed to zero-point fluctuations in the spin direction (beyond our calculations), which lower the expectation value of the onsite spin moment. This effect is especially large in $KCuF_3$, as a result of the quasi-one-dimensional nature of its magnetic structure.

Based on the spin-polarized energies given in Table III, one may derive some rough estimates for the Cu superexchange coupling constants along the *c* axis (J_c) and within the ab plane (J_a). Using an Ising model—with interactions $2J_{c(a)}S_z^{(A)}S_z^{(B)}$ between spins $S=1/2$ on adjacent A and B sites along the *c* axis (within the *ab* plane)—to map our calculated magnetic energies, we obtain for J_c values of +70 and +48 meV from the energy differences E[FM]−E[A-AF] and E[C-AF]−E[G-AF], respectively, and for J_a values of −5 and +6 meV from E[G-AF]−E[A-AF] and E[FM] −E[C-AF], respectively. Clearly, the variation in the values derived for J_c (J_a) indicates that the changes in the spin configurations that we consider are too large to be in the harmonic regime. These values, however, are nevertheless in order-of-magnitude agreement with the experimental values of $J_c=17.5$ meV and $J_a\approx -0.2$ meV.[3,20]

VI. INFLUENCE OF THE MAGNETIC STRUCTURE ON THE ORBITAL ORDERING AND JAHN-TELLER DISTORTION

In Fig. 8 we display the total energy of the various spin structures considered in the previous section as a function of the quadrupolar distortion ΔX. The calculated equilibrium distortions range from 4.65% (FM) to 5.15% (NM), with an equilibrium value of 4.8% for the A-AF structure. The

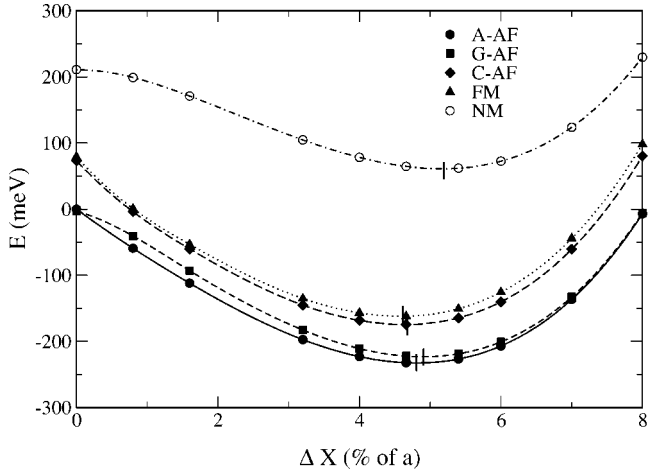

FIG. 8. Total energy of the various magnetic structures of $KCuF_3$ considered in this work as a function of the quadrupolar distortion ΔX.

changes in the spin structure induce thus variations in the Jahn-Teller distortion which do not exceed 10%. This 10% value, obtained when the NM structure is considered, is a conservative upper bound for the estimated variation in the Jahn-Teller distortion produced by the A-AF to paramagnetic transformation. Indeed, experimentally, strong antiferromagnetic spin correlations are known to persist above the Néel temperature within the Cu chains along the *c* axis. Locally, this would be more realistically described using configurations of the type G-AF and A-AF. For example, if one considers a structure composed of Cu AF chains along the *c* axis, with no interchain magnetic interaction, and uses an Ising model to describe the spin interactions, the energy of this structure is the average of the energies of the G-AF and A-AF configurations. Using such a description to model the structure above the Néel temperature, and with the energies of the G-AF and A-AF configurations given in Fig. 8, the estimated change in the Jahn-Teller distortion produced by the magnetic transformation decreases to $\sim$1%.

To compare the orbital ordering in the different spin structures, we have reported in Table IV the calculated number of $3d_{z^2-x^2}$ holes on the A site, $\overline{n}^{A,\mathrm{hole}}_{z^2-x^2}$, together with the total number of $3d$-e_g holes per Cu site, $n^{\mathrm{hole}}_{e_g}$, in each structure. These values have been calculated using the same quadrupolar distortion for all structures, i.e., $\Delta X=4.6\%$. If one uses,

TABLE IV. Calculated number of $3d$-e_g hole per Cu site, n_{e_g}, and expectation value of the number of $3d_{z^2-x^2}$ hole on a Cu A site, $\overline{n}^{A,\mathrm{hole}}_{d_{z^2-x^2}}$, in the various spin structures of $KCuF_3$ considered in this work.

	$\overline{n}^{A,\mathrm{hole}}_{z^2-x^2}$	$n^{\mathrm{hole}}_{e_g}$
A-AF	0.61	0.63
G-AF	0.62	0.63
C-AF	0.62	0.66
FM	0.64	0.66
NM	0.42	0.46

instead, the calculated equilibrium ΔX for each structure, the numbers, in Table IV, change by less than 1%. For all spin structures, the orbital ordering is almost exclusively of the z^2-x^2/z^2-y^2 type; the $d_{z^2-x^2}/d_{z^2-y^2}$ character, given by the ratio $n^{A,\mathrm{hole}}_{z^2-x^2}/n^{\mathrm{hole}}_{e_g}$, ranges from 91% for the NM structure to 98% for the G-AF structure. The major change we observe is a strong decrease ($\sim$30%) in the degree of orbital ordering, given by $\bar{n}^{A,\mathrm{hole}}_{z^2-x^2}$, of the NM structure relative to those of the other structures. This decrease is associated with an increased delocalization of the 3*d* hole. Although there is an important change thus in the orbital ordering—and 3*d* hole occupation—induced by a change from the magnetic to the NM configuration, we will see in the next section that such a change does not have a major impact on the RXS spectrum.

VII. RXS SPECTRA

Resonant elastic x-ray scattering is a second order process in which a core electron is virtually promoted to some intermediate states above the Fermi energy, and subsequently decays to the same core level. We concentrate here on RXS near the Cu *K* absorption edge, and examine the resonant scattering intensity for Bragg reflections that selectively probe the orbital order (or equivalently the Jahn-Teller structural order). The corresponding Bragg vectors are $\boldsymbol{G}=(h,k,l)$, with h,k,l odd, in units $(\pi/a,\pi/a,\pi/c)$. We consider dipole transitions to Cu 4*p* band states, and neglect the effect of the core-hole potential on the intermediate states.

The RXS intensity for a Bragg vector $\boldsymbol{Q}$ and incoming-(outgoing-) photon energy $\hbar\omega$ may be written as

$$I(\boldsymbol{G},\hbar\omega)\propto\left|\sum_j e^{i\mathbf{Q}\cdot\mathbf{R}_j}\sum_{\alpha,\beta}F^j_{\alpha,\beta}(\hbar\omega)\epsilon_\alpha\epsilon'_\beta\right|^2, \tag{3}$$

where $\boldsymbol{R}_j$ are the positions of the Cu ions in the unit cell, ϵ_α (ϵ'_β) are the components of the polarization vector of the incoming (outgoing) photon, $\alpha(\beta)=x,y,z$, and

$$F^j_{\alpha,\beta}(\hbar\omega)=\sum_{\boldsymbol{k},n}\frac{\langle\psi^{(j)}_0|r_\alpha(j)|\psi^{4p}_{\boldsymbol{k},n}\rangle\langle\psi^{4p}_{\boldsymbol{k},n}|r_\beta(j)|\psi^{(j)}_0\rangle}{\hbar\omega+E_0-E^{4p}_{\boldsymbol{k},n}-i\Gamma/2} \tag{4}$$

are the components of the resonant atomic scattering tensor for the *j*th Cu ion in the cell. In Eq. (4), $\psi^{(j)}_0$ is the Cu 1*s* wave function at site *j*, E_0 is the corresponding core level energy, $\boldsymbol{r}(j)$ is the position operator measured relative to $\boldsymbol{R}_j$, $\psi^{4p}_{\boldsymbol{k},n}$ ($E^{4p}_{\boldsymbol{k},n}$) are the empty Cu 4*p* band states (energies) with Bloch vector *k* and band index *n*, and Γ is the broadening corresponding to the inverse lifetime of the Cu 1*s* core-hole and 4*p* electron excited states.

For Bragg vectors associated with the orbital order, the structure factors, in Eq. (3), read

$$\sum_j e^{i\mathbf{Q}\cdot\mathbf{R}_j}F^j_{\alpha,\beta}=2(F^A_{\alpha,\beta}-F^B_{\alpha,\beta}), \tag{5}$$

where $F^{A(B)}_{\alpha,\beta}$ is the atomic scattering tensor of a Cu ion at site A (B), and the factor of 2 accounts for the two A (B) Cu ions in the unit cell. Because of the reflection symmetries σ_x, σ_y, and σ_z present at the Cu sites in $KCuF_3$, the only nonvanishing components of the atomic scattering tensors are $F^{A(B)}_{x,x}$, $F^{A(B)}_{y,y}$, and $F^{A(B)}_{z,z}$, and because of the 90° roto-translation symmetry that transforms the A and B sites into each other, one has: $F^A_{x,x(y,y)}=F^B_{y,y(x,x)}$ and $F^A_{z,z}=F^B_{z,z}$. The scattering intensity in Eq. (3) may therefore be written as

$$I(\boldsymbol{G},\hbar\omega)\propto|F^A_{x,x}(\hbar\omega)-F^A_{y,y}(\hbar\omega)|^2|\epsilon_x\epsilon'_x-\epsilon_y\epsilon'_y|^2. \tag{6}$$

Except for the special case where the polarization-dependent term on the right-hand side of Eq. (6) vanishes, the scattering intensity is proportional thus to $|F^A_{x,x}(\hbar\omega)-F^A_{y,y}(\hbar\omega)|^2$. We also note that, within the extremely localized core region where the Cu 1*s* wave function does not vanish, the radial dependence of each band state $\psi^{4p}_{\boldsymbol{k},n}$, in Eq. (4), is essentially the same as that of the atomic 4*p* state, except for a global scaling factor in the wave-function amplitude. The scattering factors, in Eq. (6), may therefore be written as

$$F^A_{\alpha,\alpha}(E)\propto\int_{E_F}^{\infty}\frac{d\varepsilon D^{4p}_\alpha(\varepsilon)}{E+E_0-\varepsilon-i\Gamma/2}, \tag{7}$$

where $D^{4p}_\alpha(\varepsilon)$ is the projected atomic $4p_\alpha$ density of states and E_F is the Fermi energy. Hence in our pseudopotential calculations we evaluate the orbital scattering intensity, $I_{\mathrm{orb}}(\hbar\omega)\propto|F^A_{x,x}(\hbar\omega)-F^A_{y,y}(\hbar\omega)|^2$, as a function of photon energy, directly from the partial 4*p* densities of states. The core-level energy E_0 (not computed here) is a value we adjust to align the main feature of the calculated and experimental RXS spectrum.[38]

In Fig. 9(a) we confront our calculated orbital RXS spectrum for the A-AF structure of $KCuF_3$ to the experimental spectrum [measured at the (3,3,1) orbital Bragg reflection and for a $\sigma-\pi'$ polarization]. We also reported in this figure the theoretical RXS spectrum of the NM structure, for comparison. Both spectra have been computed using the experimental values of the structural parameters. A spectrum obtained for the A-AF structure with a 50% increase in ΔX is also shown in Fig. 9(a). The corresponding calculated *K*-edge absorption spectra $A(\hbar\omega)$, evaluated as $A(\hbar\omega)\propto\mathrm{Im}[F^A_{x,x}(\hbar\omega)+F^A_{y,y}(\hbar\omega)+F^A_{z,z}(\hbar\omega)]$, are displayed in Fig. 9(b) and also compared to experiment (fluorescence data).[7] All theoretical spectra have been evaluated using for Γ 0.5 eV, and we convoluted these spectra with a Gaussian of full-width at half maximum of 1 eV.

The calculated RXS and absorption spectra for the A-AF structure are in reasonable agreement with the experimental data. We note, however, that the energy separation between the two main features in the RXS spectrum is somewhat underestimated in our calculations, and the intensity of the high-energy feature near 9 keV is also not very well reproduced (both in the RXS and in the absorption spectrum). The change in the magnetic configuration, from the A-AF structure to the NM structure, decreases somewhat the RXS intensity. We note, however, that this change is very small compared to the factor of 2 decrease in intensity observed experimentally when the material transforms to the paramagnetic phase. The weak dependence of the RXS spectrum on the magnetic configuration is consistent with the results of previous all-electron calculations for the A-AF structure (cal-

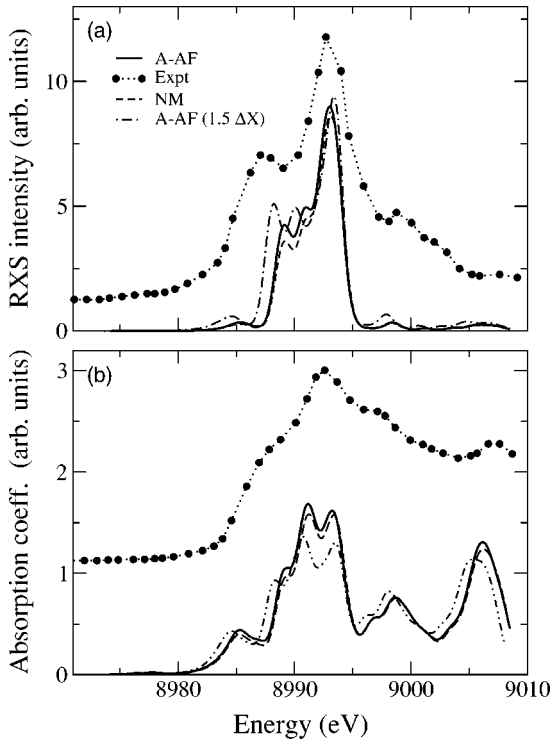

FIG. 9. Orbital RXS intensity (a) and absorption coefficient (b), as a function of photon energy, near the Cu *K* edge in $KCuF_3$. The calculated spectra of the A-AF (solid line) and NM (dashed line) structures are displayed. The effect of a 50% increase in the quadrupolar distortion, ΔX, in the A-AF structure is also shown (dashed-dotted line). The experimental data are from Ref. 7; the measured RXS spectrum corresponds to a (3,3,1) orbital Bragg reflection and a $\sigma-\pi'$ polarization.

culated within the LDA+U) and the NM structure (calculated within the LDA in previous studies).[8,18]

To assess the influence of the orbital ordering on the RXS signal, we have also computed the RXS intensity of the A-AF structure without the quadrupolar distortion ($\Delta X \sim 0$). Although the z^2-x^2/z^2-y^2 orbital ordering is still large in this case: $\bar{n}^{A,\mathrm{hole}}_{z^2-x^2}=0.64$, $n^{\mathrm{hole}}_{e_g}=0.68$, the calculated RXS signal is about two orders of magnitude smaller than that obtained with the experimental Jahn-Teller distortion; the orbital ordering by itself thus has a negligible influence on the RXS intensity. We note that the fact that $\bar{n}^{A,\mathrm{hole}}_{z^2-x^2}$ (and $n^{\mathrm{hole}}_{e_g}$) are very similar with and without the quadrupolar distortion indicates that, already at vanishing ΔX, the orbital ordering has essentially reached its saturation value, given the hybridization present in the system.

Concerning the effect of the Jahn-Teller distortion, we observe that increasing ΔX by 50% increases noticeably the splitting between the two mean features in the RXS spectrum of the A-AF structure, but does not change significantly the intensity of the dominant peak. Decreasing, instead, ΔX by the same amount has a larger influence on the RXS intensity,[18] but corresponds to a situation where the two features are essentially merged. A change in the Jahn-Teller distortion in the magnetic phase (not supported by our LDA+U calculations of the Jahn-Teller distortion) has been suggested as a possible cause of the drastic change observed experimentally in the RXS signal near the Néel temperature.[18] We observe here, however, that a factor of 2 change in the RXS intensity would require a drastic change in ΔX, in the conventional crystallographic structure of $KCuF_3$. Such a change is bound to induce also a substantial change in the c/a ratio (see Sec. III), which has not been observed experimentally. The Jahn-Teller origin of the jump in intensity appears thus somewhat unlikely. We therefore suggest that possibly a structural transformation occurs at low temperature in $KCuF_3$, which is reflected in the RXS signal. We note that such a change in the crystal structure would not be inconsistent with some unexplained Raman[39] and nuclear magnetic resonance[40] features observed experimentally at low temperature in this material. We also note that recently a new crystal structure (superstructure) has been proposed for $KCuF_3$ based on x-ray diffraction at room temperature.[41] In our LDA+U calculations, however, this structure is found to relax to the conventional crystallographic structure of $KCuF_3$.

VIII. CONCLUSIONS

We have studied by means of LDA+U pseudopotential calculations the structural, electronic, and magnetic properties of $KCuF_3$, and investigated the Cu *K*-edge RXS spectrum for Bragg reflections associated with orbital order. In our studies, we considered several different (meta)-stable spin structures for $KCuF_3$ in order to assess the influence of the magnetic structure on the orbital ordering, Jahn-Teller distortion, and RXS spectrum.

For $KCuF_3$, the LDA fails to correctly predict the stable AF insulating structure. We have found here that LDA+U pseudopotential calculations provide an accurate general description of the properties of this system. The ground state is correctly predicted to be an A-type AF structure. The structural parameters obtained from the LDA+U calculations agree also well with experiment, with an accuracy comparable to that obtained by LDA calculations for other perovskite materials. The orbital ordering is predominantly of the z^2-x^2/z^2-y^2 type, consistent with previous theoretical predictions for this system. We find, however, that the orbital-order parameter is significantly reduced with respect to its nominal value due to Cu($3d$)–F($2p$) hybridization. We also find that, given this hybridization, the Cu-$3d$ orbital ordering in the A-AF phase is already saturated at vanishing Jahn-Teller quadrupolar distortion of the F neighbors.

The RXS spectrum calculated for the A-AF structure agrees relatively well with the experimental spectrum. We find that the resonant signal is dominated by the Jahn-Teller distortion, with a minor influence of the orbital ordering, in agreement with previous theoretical results. Our LDA+U calculations, however, also indicate that a change in the magnetic structure has a small influence on the Jahn-Teller distortion, and hence on the resonant spectrum, in the commonly accepted crystallographic structure of $KCuF_3$. We therefore suggest that the change observed experimentally in

the RXS signal near the Néel temperature may be related to a low-temperature structural transformation in $KCuF_3$. We also note that preliminary results obtained from LDA+U molecular-dynamic simulations for A-AF $KCuF_3$ indicate the existence of a superstructure, with tilted CuF_6 octahedra, which is slightly lower in energy than the conventional crystal structure of $KCuF_3$.

ACKNOWLEDGMENTS

It is a pleasure to thank R. Caciuffo, S. de Gironcoli, M. Cococcioni, G. Trimarchi, and N. Stojic for useful discussions. The calculations are based on the PWSCF code.[42] We acknowledge support for this work by the INFM within the framework of the "Iniziativa Trasversale di Calcolo Parallelo."

[1] K. I. Kugel and D. I. Khomskii, Sov. Phys. JETP **37**, 725 (1973).
[2] J. B. Goodenough, *Magnetism and the Chemical Bond* (Interscience, New York, 1963).
[3] M. T. Hutchings, E. J. Samuelsen, G. Shirane, and K. Hirakawa, Phys. Rev. **188**, 919 (1969).
[4] For a theoretical overview of the role of orbital degeneracy in cuprates and manganites, see e.g., A. M. Oleś, M. Cuoco, and N. B. Perkins, in *Lectures on the Physics of Highly Correlated Electron Systems IV*, edited by F. Mancini, AIP Conf. Proc. No. 527 (AIP, Melville, NY, 2000), p. 226 .
[5] Y. Murakami, J. P. Hill, M. Blume, I. Koyama, M. Tanaka, H. Kawata, T. Arima, Y. Tokura, K. Hirota, and Y. Endoh, Phys. Rev. Lett. **81**, 582 (1998).
[6] M. v. Zimmermann, C. S. Nelson, J. P. Hill, D. Gibbs, M. Blume, D. Casa, B. Keimer, Y. Murakami, C. C. Kao, C. Venkataraman, T. Gog, Y. Tomioka, and Y. Tokura, Phys. Rev. B **64**, 195133 (2001), and references therein.
[7] L. Paolasini, R. Caciuffo, A. Sollier, P. Ghigna, and M. Altarelli, Phys. Rev. Lett. **88**, 106403 (2002).
[8] R. Caciuffo, L. Paolasini, A. Sollier, P. Ghigna, E. Pavarini, J. van den Brink, and M. Altarelli, Phys. Rev. B **65**, 174425 (2002).
[9] S. B. Wilkins, P. D. Hatton, M. D. Roper, D. Prabhakaran, and A. T. Boothroys, Phys. Rev. Lett. **90**, 187201 (2003).
[10] S. B. Wilkins, P. D. Spencer, P. D. Hatton, S. P. Collins, M. D. Roper, D. Prabhakaran, and A. T. Boothroys, Phys. Rev. Lett. **91**, 167205 (2003); S. B. Wilkins (private communication).
[11] S. S. Dhesi, A. Mirone, C. De Nadai, P. Ohresser, P. Bencok, N. B. Brookes, P. Reuter, A. Revcolevschi, A. Tagliaferri, O. Toulemonde, and G. van der Laan, Phys. Rev. Lett. **92**, 056403 (2004).
[12] K. J. Thomas, J. P. Hill, Y. J. Kim, S. Grenier, P. Abbamonte, L. Venema, A. Rusydi, Y. Tomioka, Y. Tokura, D. F. McMorrow, and M. van Veenendaal, cond-mat/0311553.
[13] S. Ishihara and S. Maekawa, Phys. Rev. Lett. **80**, 3799 (1998).
[14] I. S. Elfimov, V. I. Anisimov, and G. A. Sawatzky, Phys. Rev. Lett. **82**, 4264 (1999).
[15] M. Benfatto, Y. Joly, and C. R. Natoli, Phys. Rev. Lett. **83**, 636 (1999).
[16] S. Di Matteo, T. Chatterji, Y. Joly, A. Stunault, J. A. Paixao, R. Suryanarayanan, G. Dhalenne, and A. Revcolevschi, Phys. Rev. B **68**, 024414 (2003), and references therein.
[17] P. Benedetti, J. van den Brink, E. Pavarini, A. Vigliante, and P. Wochner, Phys. Rev. B **63**, 060408(R) (2001).
[18] M. Takahashi, M. Usuda, and J. Igarashi, Phys. Rev. B **67**, 064425 (2003).
[19] A. Okazaki, J. Phys. Soc. Jpn. **26**, 870 (1969).
[20] S. K. Satija, J. D. Axe, G. Shirane, H. Yoshizawa, and K. Hirakawa, Phys. Rev. B **21**, 2001 (1980).
[21] A. I. Liechtenstein, V. I. Anisimov, and Z. Zaanen, Phys. Rev. B **52**, R5467 (1995).
[22] M. D. Towler, R. Dovesi, and V. R. Saunder, Phys. Rev. B **52**, 10 150 (1995).
[23] J. E. Medvedeva, M. A. Korotin, V. I. Anisimov, and A. J. Freeman, Phys. Rev. B **65**, 172413 (2002).
[24] M. Cococcioni, Ph.D. thesis, SISSA, 2002, http://www.sissa.it/cm/phd.php; M. Cococcioni and S. de Gironcoli, cond-mat/0405160.
[25] H. Sawada, Y. Morikawa, K. Terakura, and N. Hamada, Phys. Rev. B **56**, 12 154 (1997).
[26] A tight-binding Bloch state, normalized over the crystal unit cell, is generated for each localized atomic function $\varphi_m^{I,\sigma}(\boldsymbol{r})$ and used to perform the projection. We note that with the ultrasoft-pseudopotential scheme, the projection includes also the augmentation pseudo-charge density (see Ref. 24).
[27] J. P. Perdew and A. Zunger, Phys. Rev. B **23**, 5048 (1981).
[28] D. Vanderbilt, Phys. Rev. B **41**, 7892 (1990).
[29] N. Troullier and J. L. Martins, Phys. Rev. B **43**, 1993 (1991).
[30] L. Kleinman and D. M. Bylander, Phys. Rev. Lett. **48**, 1425 (1982).
[31] S. G. Louie, S. Froyen, and M. L. Cohen, Phys. Rev. B **26**, 1738 (1982).
[32] H. J. Monkhorst and J. D. Pack, Phys. Rev. B **13**, 5188 (1976).
[33] C.-L. Fu and K.-M. Ho, Phys. Rev. B **28**, 5480 (1983).
[34] R. D. King-Smith and D. Vanderbilt, Phys. Rev. B **49**, 5828 (1994).
[35] R. H. Buttner, E. N. Maslen, and N. Spadaccini, Acta Crystallogr., Sect. B: Struct. Sci. **46**, 131 (1989).
[36] A. E. Nikiforov and S. Y. Shaahkin, Phys. Solid State **38**, 1880 (1996).
[37] The projected atomic DOS are evaluated from projections within a small atomic-core sphere: $\int d\Omega \int_0^{\mathrm{rmax}} dr r^2 \varphi_m^*(\boldsymbol{r}) \psi_{\boldsymbol{k},i}(\boldsymbol{r})$, where rmax=0.5 a.u. Changing rmax to 1 a.u. or. 0.2 a.u. leaves the projected DOS unchanged (except for a constant scaling factor).
[38] We note that an accurate determination of the absolute value of the Cu $1s^2, 4p^0 \rightarrow$ Cu $1s^1, 4p^1$ excitation energy is presently beyond the reach of state-of-the-art *ab initio* all-electron LDA computations (see, e.g., Ref. 18).
[39] T. Ueda, K. Sugawara, T. Kondo, and I. Yamada, Solid State Commun. **80**, 801 (1991).
[40] C. Mazzoli, G. Allodi, R. De Renzi, G. Guidi, and P. Ghigna, J. Magn. Magn. Mater. **242**, 935 (2002).
[41] M. Hidaka, T. Eguchi, and I. Yamada, J. Phys. Soc. Jpn. **67**, 2488 (1998).
[42] S. Baroni, A. Dal Corso, S. de Gironcoli, and P. Giannozzi, http://www.pwscf.org